ACS APPLIED NANO MATERIALS

www.acsanm.org Article

Fundamental Skeletal Nanostructure of Nanoporous Polymer-Cross-Linked Alginate Aerogels and Its Relevance To Environmental Remediation

Patrina Paraskevopoulou,* Grigorios Raptopoulos, Adél Len, Zoltán Dudás, István Fábián, and József Kalmár*

Cite This: https://doi.org/10.1021/acsanm.1c02072 Read Online

ACCESS | Metrics & More | Article Recommendations

ABSTRACT: Nanoporous polyurea-cross-linked Ca-alginate (X-Ca-alginate) aerogels were prepared by reacting an aliphatic or aromatic triisocyanate with the preformed biopolymer network post gelation and drying in supercritical CO_2. The nanomorphology of native Ca-alginate aerogels together with those of the different X-Ca-alginate aerogels were investigated using low-voltage scanning electron microscopy, N_2-sorption porosimetry, and contrast variation small-angle neutron scattering. Native Ca-alginate aerogels were built from primary nanoparticles (8.3 ± 0.1 nm in radius) that attach to one another forming secondary particles. In X-Ca-alginate aerogels, the aliphatic and aromatic polyureas attach to primary nanoparticles (which increase in size up to 10.0 ± 0.1 nm) via urethane linkages, and then they extend into the empty space within secondary particles in different ways. Cross-linking with an aliphatic triisocyanate leads to the formation of a dense polyurea layer over the primary nanoparticles, following the contours of the Ca-alginate skeletal framework. The rigid aromatic triisocyanate forms a more loose and randomly oriented polymer structure that more or less fills the empty space between the primary nanoparticles within the secondary particles. Both processes leave the primary Ca-alginate structure practically undisturbed, while it does affect the structure at the most fundamental level, increasing the primary particle size and reducing the porosity. The different fundamental skeletal nanostructures of X-Ca-alginate aerogels affect not only their material properties but also their potential for application in environmental remediation.

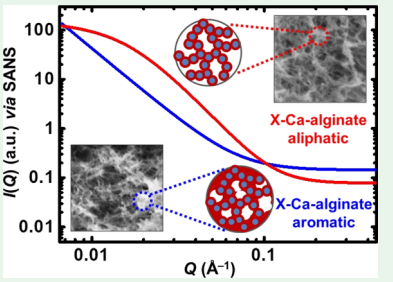

KEYWORDS: *aerogel, cross-linking, polyurea, isocyanate, alginate, SANS*

INTRODUCTION

Aerogels are solid colloidal or polymeric networks of nanoparticles expanded throughout their entire volume by a gas.[1,2] Silica aerogels were the first example of this class of nanostructured materials and were prepared in early 1930s by Kistler,[3] followed by a wide range of other inorganic oxide aerogels and later by organic (organic polymer or biopolymer-based), hybrid organic−inorganic, and carbon aerogels.[4] The diversity of the chemical composition, along with specific properties related to their nanoporous structure (high surface areas, low thermal conductivities, low dielectric constants, and high acoustic attenuation), has led to the development of numerous applications for aerogels in the fields of energy (e.g., thermal insulation and batteries), catalysis, biosciences, environmental remediation, sensors, or the food industry,[4] with thermal insulation being the most common among them.[5]

One issue that had to be overcome for the practical application of aerogels was the enhancement of their mechanical strength, as many of them, that is, most of inorganic and biopolymer aerogels, are mechanically weak and fragile materials. That issue was addressed initially for inorganic aerogels[6−15] and more recently also for biopolymer aerogels[16−18] by the development of the polymer-cross-linking (X-aerogel) technology. This involves reaction of functional groups (e.g., −OH or $-NH_2$) present on the surface of preformed wet gel networks with multifunctional reagents (e.g., multifunctional isocyanates), thus coating and cross-linking the entire (inorganic or biopolymer) network of the gel with a nanothin polymeric layer. In the case of X-biopolymer (X-alginate and X-chitosan) aerogels, an aliphatic or aromatic triisocyanate reacts with the biopolymer network post gelation.[16−18] The triisocyanate first reacts with the −OH or $-NH_2$ groups available on the surface of the biopolymer network and attaches to it through urethane or urea linkages. Subsequently, it reacts with water adsorbed on the biopolymer network and forms a polyurea film that coats the

Received: July 21, 2021
Accepted: September 14, 2021

https://doi.org/10.1021/acsanm.1c02072
ACS Appl. Nano Mater. XXXX, XXX, XXX−XXX

Scheme 1. Structures of Calcium Alginate (Ca-Alginate) and of the Triisocyanates Desmodur N3300 (Trimer of Hexamethylene Diisocyanate) and Desmodur RE (TIPM); Ca-Alginate is a Block Copolymer of β-(1 → 4)-Linked D-Mannuronate (M) and α-(1 → 4)-Linked L-Guluronate (G)[52]

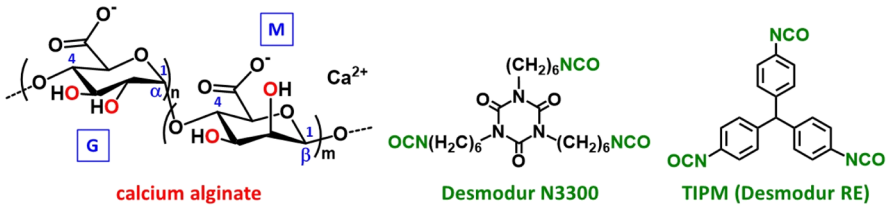

biopolymer network. The high mechanical strength and hydrophobicity of these materials render them good candidates for several applications, including drug delivery and environmental remediation. Indeed, X-alginate aerogels have been successfully used as adsorbents of Pb^{2+} ions, organic solvents, and oils from seawater.[19]

Another parameter that plays a crucial role for the adoption of aerogels in practical use is their nanoporous structure, which depends on the spatial relationship of primary and secondary particles, which in turn depends on the drying method. Primary nanoparticles are the smallest, most fundamental, dense particles on the skeletal framework of a wet gel. Primary particles form nanoporous mass-fractal aggregates, which are referred to as secondary particles. Secondary particles are connected to each other with covalent bonds and form the skeletal network of the wet gel. The pore sizes of that network are often in the range of mesopores (2−50 nm), while micropores (<2 nm) as well as small (50−300 nm) and larger macropores (>300 nm) might also be present.[4] However, this network can easily collapse during drying. To avoid such collapse, the best drying method has proven to be drying with a supercritical fluid (pure CO_2 or solvent/CO_2 mixtures).[20−24]

The nanoporous structure of aerogels can be probed with several techniques, such as porosimetry (using N_2, Ar, CO_2, or Hg), pycnometry (using He), or scanning electron microscopy (SEM).[4] Small angle X-ray scattering (SAXS) and small-angle neutron scattering (SANS) can also yield structural information on hybrid and composite materials, such as aerogels, if the fundamental building blocks are nanometer-sized. Several SAXS and SANS studies on aerogels with different chemical compositions, including silica,[25−29] carbon,[30−36] organic polymer,[37−45] biopolymer,[46] or hybrid[9,47−51] aerogels, have been reported in the literature. These studies have proved the presence of nanometer-sized primary particles.

In this work, we report the in-depth structural characterization, including a SANS study, of X-Ca-alginate aerogels prepared by cross-linking Ca-alginate wet gels with the aliphatic triisocyanate Desmodur N3300 or the aromatic triisocyanate Desmodur RE (Scheme 1). Apart from the difference in the chemical composition of the two triisocyanates, leading to an aliphatic or aromatic polyurea network, respectively, another significant difference is the relative flexibility of the two triisocyanates and the corresponding polyureas. The polyurea based on Desmodur N3300 is aliphatic and flexible, while the polyurea based on Desmodur RE is aromatic and rigid.

The ultimate goal of this study was to investigate the relation of the Ca-alginate and the polyurea components as the structural elements of the composite X-Ca-alginate aerogel architectures. It was shown that due to the difference in the relative flexibility of the polyureas, the two different X-Ca-alginate aerogels display characteristically different nanoscale morphologies.

EXPERIMENTAL SECTION

Materials and Methods. Sodium alginate was purchased from Acros Organics. Sodium alginate is a block copolymer of β-(1 → 4)-linked D-mannuronate (M) and α-(1 → 4)-linked L-guluronate (G) (41% G and 59% M; G/M ratio: 0.69). $CaCl_2 \cdot 2H_2O$ (>99%) was purchased from Fisher Scientific. Desmodur Ultra N3300 (trimer of hexamethylene diisocyanate, an aliphatic triisocyanate) and Desmodur RE [27% w/w triphenylmethane-4,4′,4″-triisocyanate (TIPM, an aromatic triisocyanate) solution in ethyl acetate] were generously provided by Covestro AG. MeCN (HPLC grade) was purchased from Fisher Scientific, acetone (P.A., ISO reagent) was purchased from Lach-Ner, and they were used as received.

Supercritical fluid drying was carried out in a pressure vessel as described before.[17,18]

Synthesis of Ca-Alginate Aerogel Beads. Native Ca-alginate (also referred to as Ca-alg) wet gel and aerogel beads were prepared following our previously published procedures.[17,18] The concentration of the starting sodium alginate solution was 2% w/w.

Synthesis of X-Ca-Alginate Aerogel Beads. X-Ca-alginate (also referred to as X-Ca-alg-N3300 or X-Ca-alg-RE) wet gel and aerogel beads were prepared following our previously published procedures.[17,18]

Characterization Techniques. The chemical identity of the X-Ca-alginate aerogel beads was confirmed with attenuated total reflection Fourier transform infrared (ATR−FTIR) spectroscopy. ATR−FTIR spectra were obtained with a PerkinElmer Spectrum 100 spectrometer.

N_2-sorption and CO_2-adsorption measurements were made on a Micromeritics Tristar II 3020 surface area and porosity analyzer (Micromeritics, Norcross, GA, USA). Skeletal densities (ρ_s) were determined by He pycnometry using a Micromeritics AccuPyc II 1340 pycnometer (Micromeritics, Norcross, GA, USA). Bulk densities (ρ_b) of the samples were calculated from their weight and natural dimensions.

The morphology of the aerogel samples was studied by low-voltage SEM (LV SEM) with a Thermo Fisher Scientific Scios 2 instrument. The samples were fixed with a vacuum-resistant carbon tape on the sample holder. Because of the low accelerating voltage and the small electron beam current, the charging effects of the aerogel sample were practically eliminated. Therefore, fresh fracture surfaces of the aerogels were imaged in their pristine states in high magnification without the application of any conductive coating on the samples.[53]

SANS. SANS experiments were performed on the Yellow Submarine instrument available at Budapest Neutron Centre (Hungary), as described in previous publications.[46,51] Two sample-to-detector distances (1.2 and 5.4 m) and two wavelengths (4.38 and 10.23 Å) were used. The momentum transfer (Q) is defined by the following equation

$$Q = \frac{4\pi}{\lambda} \sin \frac{\theta}{2} \quad (1)$$

Here, λ is the wavelength of the monochromatic neutron beam and θ is the scattering angle. By altering λ and the sample-detector distance, a Q range of 0.007−0.400 $Å^{-1}$ was covered. The definition of the scattering intensity (I) is as follows

https://doi.org/10.1021/acsanm.1c02072
ACS Appl. Nano Mater. XXXX, XXX, XXX−XXX

Scheme 2. Reaction Scheme Showing the Cross-linking of Ca-Alginate Wet Gels with the Triisocyanates Desmodur N3300 (Aliphatic) or Desmodur RE (Aromatic)

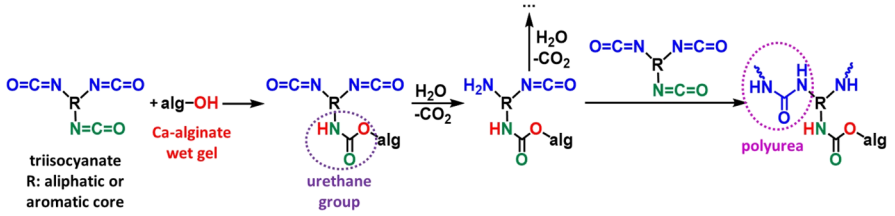

$$I(\lambda, \theta) = I_0(\lambda)\Delta\Omega\eta(\lambda)TV\frac{d\Sigma}{d\Omega}(Q) \quad (2)$$

Here, I_0 is the incoming neutron flux, $\Delta\Omega$ is the unit solid angle, $\eta(\lambda)$is the detector efficiency, and T and V are the transmission and volume of the sample. $\frac{d\Sigma}{d\Omega}(Q)$ is the macroscopic differential cross section, which conveys structural information on the studied system. The measured scattering intensity was corrected for sample transmission, empty cell scattering, solvent scattering, detector sensitivity, and background scattering.

The structural parameters of the scattering objects were determined by the mathematical analysis of the corrected $I(Q)$ curves. In general, the Guinier and Porod approximations can be used for fitting different parts of SANS curves. Their combination is referred to as the Beaucage model.[54,55] This unified model is applicable to describe the whole measured Q range in the case of the present results, as will be discussed later.

$$I(Q) \cong A\exp\left(-\frac{Q^2R_g{}^2}{3}\right) + B\left\{\frac{\left[\mathrm{erf}\left(\frac{QR_g}{\sqrt{6}}\right)\right]^3}{Q}\right\}^{-p} \quad (3)$$

R_g is the average gyration radius, p is the Porod power exponent, and A and B are coefficients related to the volume and number density of the scattering objects and to their contrast. Parameters A and B can be treated as adjustable scaling parameters. Data fitting was performed by using nonlinear least-squares algorithms in the Igor Pro 6.1 software.[56]

First, dry as-prepared (pristine) Ca-alginate or X-Ca-alginate aerogel beads were tightly packed into 5.0 mm thick quartz cuvettes and measured without any pretreatment. Subsequently, the same samples were filled with a H_2O–D_2O mixture of 46 wt % H_2O–54 wt % D_2O (49–51 V %) to a water/dry aerogel mass ratio of 5.0 g/g. This H_2O–D_2O mixture was used in order to match the contrast of the native Ca-alginate, as will be discussed later. The filled samples were stored overnight at room temperature before SANS measurements. The SANS experiments were realized in 60–180 min in room temperature using 8.0 mm beam diameter.

RESULTS AND DISCUSSION

Ca-alginate wet gels were cross-linked with an aliphatic (Desmodur N3300) or aromatic (Desmodur RE) triisocyanate (Scheme 1) following recent literature procedures.[17,18] In brief, Ca-alginate wet gels, prepared by gelation of sodium alginate with Ca^{2+}, were kept in a solution of triisocyanate. Triisocyanate diffused into the pores of the wet gels, and the cross-linking reaction was completed in an oven at 70 °C. The mechanism of the reaction has been published before[16] and is summarized in Scheme 2. One –NCO group of the triisocyanate reacts with the –OH groups of the alginate backbone forming a urethane linkage to the surface. The remaining –NCO groups of the triisocyanate are hydrolyzed to $-NH_2$ by water from the sol that has remained adsorbed on the surface of the alginate wet gel network. The alginate backbone has several functional groups (–OH, $-COO^-$) capable of hydrogen bonding with water.[57]

The $-NH_2$ groups react with triisocyanate molecules in the pores and form urea groups. Hydrolysis of the new dangling –NCO groups continues, followed by reaction of new dangling $-NH_2$ groups with fresh triisocyanate molecules in the pores, and the Ca-alginate network gets cross-linked with polyurea.

The two X-Ca-alginate aerogels were characterized with ATR–FTIR (Figure 1). The spectra confirmed the formation of both the aliphatic and aromatic polyurea, in agreement with previous results.[17,18] In brief, they show all characteristic peaks of native Ca-alginate (e.g., the asymmetric and symmetric stretching vibrations of $-COO^-$ groups coordinated to Ca^{2+} ions at 1603 and 1419 cm^{-1} and the stretching vibrations of the C–O–C groups on the sugar ring at 1082 and 1032 cm^{-1}) plus characteristic peaks attributed to polyurea. More specifically, they show the stretching vibrations of the urea –C=O (around 1630 cm^{-1} for the aliphatic and 1660 cm^{-1} for the aromatic polyurea) and the scissoring vibrations of the urea N–H (around 1530 cm^{-1} for the aliphatic and 1560 cm^{-1} for the aromatic polyurea). The stretching vibration of the urethane –C=O is visible as a shoulder around 1720 cm^{-1} in the spectrum of X-Ca-alg-RE. No peaks are observed at 2266 cm^{-1} (the vibration of –N=C=O), showing that there are practically no unreacted isocyanate groups.

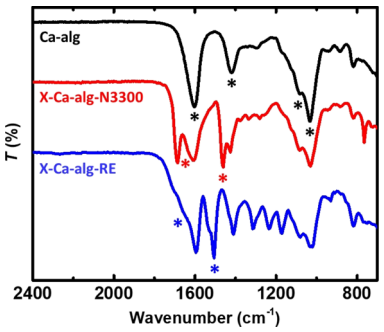

Figure 1. ATR–FTIR spectra of native (Ca-alg) and cross-linked (X-Ca-alg-N3300 and X-Ca-alg-RE) aerogels, as indicated. Characteristic peaks are discussed in the text and are marked in the figure with asterisks.

Selected material properties are reported in Table 1 and they are also in agreement with our previous reports.[17,18] The polyurea content, calculated from the skeletal densities of native and cross-linked samples,[17,18] is about the same: 56% w/w for X-Ca-alg-N3300 and 60% w/w for X-Ca-alg-RE. The N_2-sorption isotherms (Figure 2) have a small loop and do not reach saturation, indicating macroporous/mesoporous materials. The Barrett–Joyner–Halenda (BJH) curves (Figure 2) for pores in the range of 1.7–300 nm show maxima at 33–35 nm for all three materials and broad distributions. The Brunauer–Emmett–Teller (BET) surface area of X-Ca-alginate aerogels is lower

https://doi.org/10.1021/acsanm.1c02072
ACS Appl. Nano Mater. XXXX, XXX, XXX–XXX

Table 1. Selected Material Properties of Native (Ca-alg) and Cross-linked (X-Ca-alg-N3300 and X-Ca-alg-RE) Aerogels

sample[a]	bulk density ρ[b] (g cm^{-3})	skeletal density ρ_s (g cm^{-3})	porosity[b] Π (% v/v)	BET surf. area σ (m^2 g^{-1}) [micropore surf. area][c]	V_{Total}[d] ($V_{1.7-300nm}$)[e] (cm^3 g^{-1})	Av. pore diam.[f] (nm)	particle radius[g] r (nm)
Ca-alg	0.076 ± 0.006	1.89 ± 0.02	96	485 [81]	13 (1.9)	16 (104)	3.3 (3.9)
X-Ca-alg-N3300	0.19 ± 0.02	1.432 ± 0.009	87	265 [0]	4.6 (1.5)	23 (69)	7.9 (7.9)
X-Ca-alg-RE	0.18 ± 0.02	1.44 ± 0.01	88	425 [49]	4.9 (1.9)	19 (46)	4.9 (5.5)

[a]The concentration of the initial sodium alginate solution was 2% w/w. [b]Porosity calculated according to the formula $(\rho_s - \rho_b)/\rho_s$, where ρ_s is the skeletal density and ρ_b is the bulk density. [c]Micropore surface area *via* *t*-plot analysis according to the Harkins and Jura model. [d]Total pore volume calculated according to the formula $1/\rho_b - 1/\rho_s$. [e]Cumulative volume of pores between 1.7 and 300 nm from N_2-sorption data and the BJH desorption method. [f]Calculated by the $4V/\sigma$ method; V was set equal to the maximum volume of N_2 adsorbed along the isotherm as $P/P_o \rightarrow 1.0$. For the number in parentheses, V was set equal to V_{total} from the previous column. [g]Particle radius calculated by the formula $r = 3/(\rho_s \times \sigma)$, where σ is the BET surface area. For the number in parentheses, σ was set equal to the external surface area, σ_{ext}, calculated from the BET surface area minus the micropore surface area.

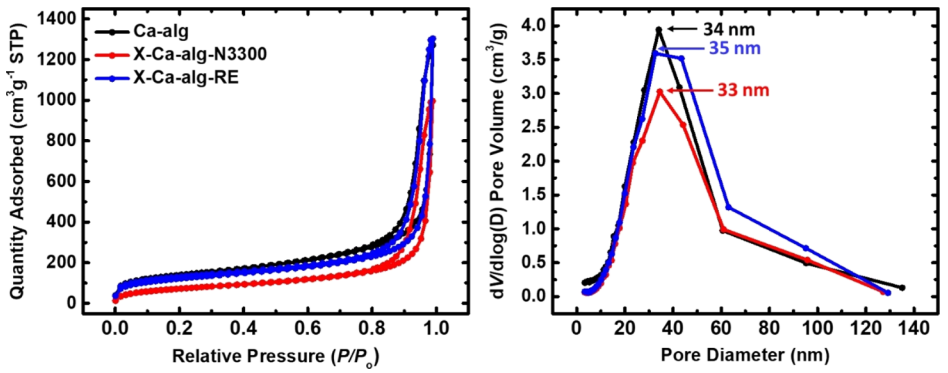

Figure 2. N_2-sorption diagrams (left) and pore size distributions by the BJH method (right) of native (Ca-alg) and cross-linked (X-Ca-alg-N3300 and X-Ca-alg-RE) aerogels, as indicated.

compared to that of the native Ca-alginate aerogels, suggesting that accumulation of polyurea evens out finer features along the skeletal framework. Fractal dimensions calculated from the N_2-sorption data were practically the same for the three samples: Ca-alg: 2.66, X-Ca-alg-N3000: 2.59, and X-Ca-alg-RE: 2.67.

Representative SEM images are shown in Figure 3 for the three aerogels. The general fibrous morphology of all aerogels in this study is traced back to the native Ca-alginate aerogels. As indicated by SANS studies below, the fibers of the native Ca-alginate aerogels are built from secondary particles that in turn are mass-fractal aggregates of primary nanoparticles. Mesoporosity corresponds to the void space among particles. As seen in the SEM images, fiber entanglement creates macropores. The morphology of the cross-linked X-Ca-alginate aerogels is practically the same as that of the native Ca-alginate aerogels. Upon closer inspection, the fibrils that form the skeletal framework of all three materials have the same aspect ratio and consist of strings of tiny beads, presumably secondary particles.

The SANS curves of the three aerogels are shown in Figure 4. For every one of the three materials, the scattering curve of the pristine aerogel and that of the same aerogel filled with the H_2O–D_2O mixture are overlaid in the same panel. The best fits using the Beaucage model are also displayed in Figure 4, and the estimated structural parameters are given in Table 2. The scattering curves of the H_2O–D_2O-filled Ca-alg and X-Ca-alg-RE samples feature only power-law type scattering and were fitted accordingly. The geometry of the network building blocks was approximated with spheres, and particle radii ($r_{particle}$) were calculated from the estimated radii of gyration (R_g) using eq 4.[54] The calculated particle sizes of the pristine aerogels are in reasonably good agreement with the values calculated from the skeletal density and N_2-sorption data (Table 2). Indeed, the assumptions entering these calculations are related to the presence of microporosity and lead to calculated radii somewhat smaller than the actual particle sizes. Supporting evidence for this argument is the case of X-Ca-alg-N3300 aerogels, which have no microporosity, and therefore the particle radii calculated with the two methods are in complete agreement with one another.

$$r_{particle}^{\ 2} = \frac{5}{3} R_g^{\ 2} \quad (4)$$

The neutron scattering length density of native Ca-alginate aerogels was calculated based on their chemical formula $[(C_{12}H_{14}CaO_{12})_n]$ and their skeletal density (1.89 cm^3 g^{-1}; Table 2), and it was found equal to 2.968×10^{-6} Å^{-2}. Therefore, the contrast of the Ca-alginate component is expected to be matched by completely filling the samples with the 46 wt % H_2O–54 wt % D_2O mixture. The calculation of that ratio was based on recently reported SANS contrast variation data.[58] Indeed, the filled Ca-alg and X-Ca-alg-RE samples show very minor specific scattering caused by nanosized objects (Figure 4). This means that the scattering of the Ca-alginate backbone is almost completely matched. Both SANS curves show a power-law behavior characteristic to mass fractals. However, it is also noted that the fitted curves deviate slightly from the experimental points. This feature might indicate the somewhat incomplete filling of pores due to hydrophobic spots or a small number of closed pores.

The shapes of the SANS curves of the pristine and H_2O–D_2O-filled X-Ca-alg-N3300 samples are similar, which indicates that contrast matching was not realized in this case.

According to the SEM images and SANS data, the fundamental fibrous structure of Ca-alginate aerogels consist of hierarchical primary and mass-fractal secondary particles.

https://doi.org/10.1021/acsanm.1c02072
ACS Appl. Nano Mater. XXXX, XXX, XXX–XXX

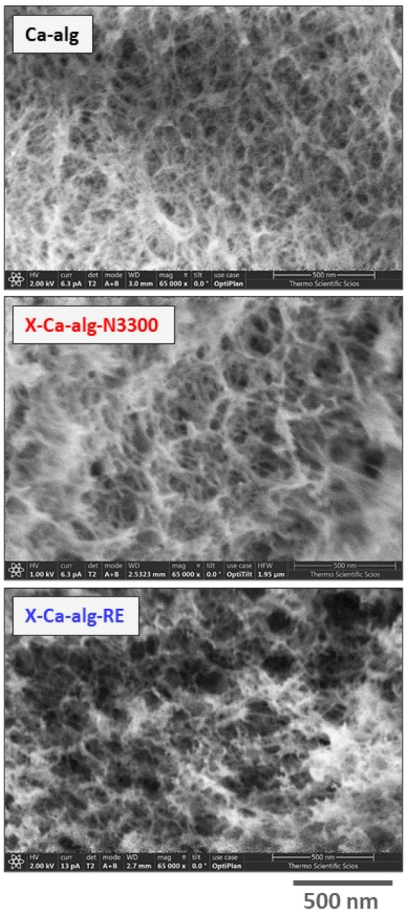

Figure 3. Representative LV SEM images of fresh-fracture surfaces of native (Ca-alg) and cross-linked (X-Ca-alg-N3300 and X-Ca-alg-RE) aerogels, as indicated.

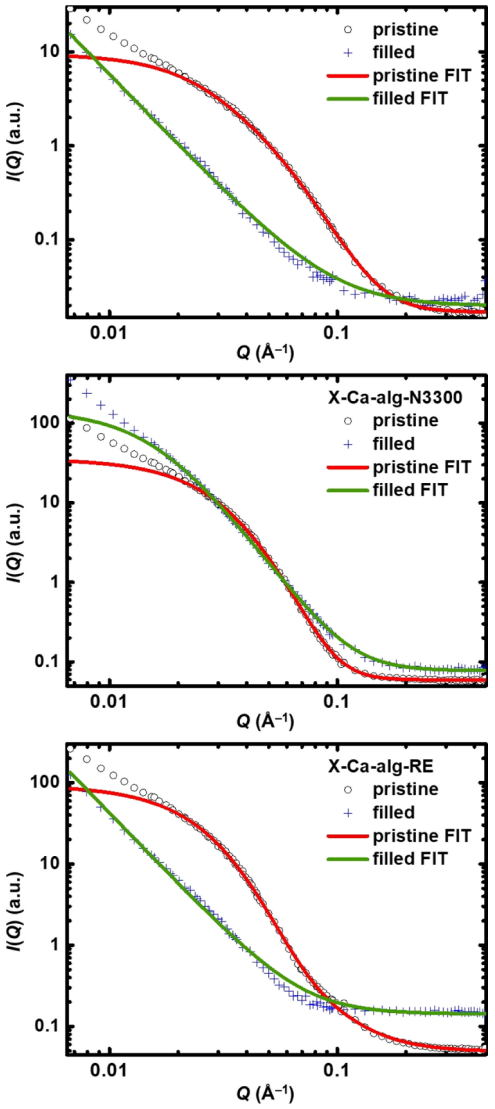

Figure 4. SANS curves of native (Ca-alg) and cross-linked (X-Ca-alg-N3300 and X-Ca-alg-RE) aerogels, as indicated. Pristine aerogels were measured first, and the same samples were filled with a H_2O-D_2O mixture of 46 wt % H_2O–54 wt % D_2O and measured again. Continuous lines are results of nonlinear model fitting. Estimated structural parameters are given in Table 2.

Fibrous aerogels consisting of such nanostructural elements have also been reported in the cases of certain polyurea and polyimide aerogels and have been described as the consequence of phase separation during the sol–gel process, yielding solid primary nanoparticles that assemble with one another following a diffusion-limited cluster aggregation mechanism.[40,42] According to these considerations, the proposed nanoscale structure of native Ca-alginate aerogels and the illustration of the principal idea behind contrast matching in SANS are shown in Figure 5.

It is reasonable to assume that the difference in the SANS contrast matching in the case of the two X-Ca-alginate aerogels indicates different relationships of the Ca-alginate and the polyurea structural elements in the two aerogel nanoarchitectures.[59] Contrast matching in the case of X-Ca-alg-N3300 aerogels can be incomplete because the flexible/aliphatic polyurea forms a more compact (with less free volume) coating on the primary Ca-alginate nanoparticles. This closer association and the interfacial covalent connectivity of the two polymers change the scattering length density of the X-Ca-alg-N3300 backbone compared to that of the native Ca-alginate.[51,60] In the case of X-Ca-alg-RE aerogels, the observations can be interpreted by assuming that the rigid/aromatic polyurea does not coat Ca-alginate as compactly as its flexible/aliphatic polyurea counterpart but rather loosely fills the space between primary particles. Using the same principles as for the illustration of the nanostructure of native Ca-alginate aerogels, the proposed nanoscale structures of X-Ca-alg-N3300 and X-Ca-alg-RE aerogels are shown in Figure 6.

The mechanistic interpretation for the formation of different nanostructures of X-Ca-alginate aerogels can be traced to the different reactivity/molecular rigidity of the two triisocyanate cross-linkers. The aliphatic triisocyanate (Desmodur N3300) reacts slower with water (and alcohols) than the aromatic triisocyanate (Desmodur RE). The slower reaction of Desmodur N3300 probably leads to the formation of a polyurea layer over the skeletal particles that follows the contours of the native Ca-alginate skeletal framework better. The flexible structure of Desmodur N3300 corroborates with this hypothesis in contrast to the rigid/aromatic structure of the polyurea from Desmodur RE triisocyanate. Thus, the more rigid Desmodur RE reacts faster and forms a more randomly oriented polymer structure, which is more prone to imperfections, leading to a longer extension of the polymer in the empty space between the

https://doi.org/10.1021/acsanm.1c02072
ACS Appl. Nano Mater. XXXX, XXX, XXX–XXX

Table 2. Structural Parameters Estimated by Fitting the SANS Curves of the Pristine and Filled Native (Ca-alg) and Cross-linked (X-Ca-alg-N3300 and X-Ca-alg-RE) Aerogels, and Particle Radii Calculated from N_2 Sorption and Skeletal Density Data (Also Shown in Table 1)[a]

sample	Beaucage model R_g (Å)	$r_{particle}$ [b] (nm)	particle radius[c] r (nm)	Beaucage model p	power-law model p
Ca-alg pristine	64 ± 1	8.3 ± 0.1	3.3 (3.9)	4.55 ± 0.03	
X-Ca-alg-N3300 pristine	68 ± 1	8.8 ± 0.1	7.9 (7.9)	5.63 ± 0.17	
X-Ca-alg-RE pristine	79 ± 1	10.0 ± 0.1	4.9 (5.5)	2.94 ± 0.03	
Ca-alg filled					2.49 ± 0.01
X-Ca-alg-N3300 filled	122 ± 4	16 ± 0.5		3.80 ± 0.03	
X-Ca-alg-RE filled					2.90 ± 0.01

[a]The SANS curves and nonlinear fits are shown in Figure 4. [b]Particle radii calculated from SANS data using eq 4. [c]Particle radii calculated by the formula $r = 3/(\rho_s \times \sigma)$, where σ is the BET surface area and ρ_s is the skeletal density. For the number in parentheses, σ was set equal to the external surface area, σ_{ext}, calculated from the BET surface area minus the micropore surface area. Values are taken from Table 1.

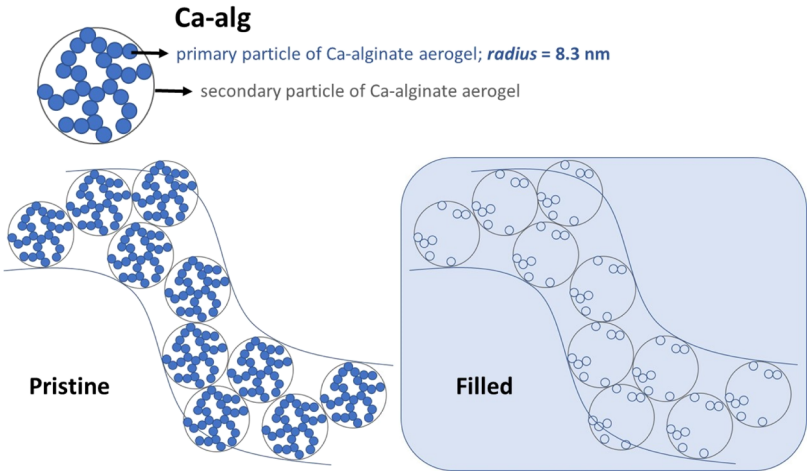

Figure 5. Proposed nanoscale structure of the native Ca-alginate (Ca-alg) aerogel. The panel labeled "filled" denotes filling with a contrast matching agent (a H_2O–D_2O mixture of 46 wt % H_2O–54 wt % D_2O) in SANS.

primary nanoparticles (within secondary particles), which may also lead to minor closed porosity.

Fractal dimensions calculated from N_2-sorption data are practically equal for the three samples (Ca-alg: 2.66, X-Ca-alg-N3000: 2.59, and X-Ca-alg-RE: 2.67) and agree well with the p value obtained by SANS for the pristine X-Ca-alg-RE aerogel (p = 2.94) and are characteristic for mass fractals. However, the p value for the pristine X-Ca-alg-N3300 aerogel is larger than 4, which indicates a gradual density change on the nanointerfaces of the cross-linked aerogel. This agrees with the fact that the nanoparticle network of all samples was formed first from Ca-alginate and that polyurea accumulated in the second step on the reactive ends of primary nanoparticles of the network by different mechanisms. The cross-linking process leaves the general aerogel architecture practically undisturbed, while it does affect the structure at the most fundamental level, increasing the primary particle size and reducing the porosity.

The different fundamental skeletal nanostructures of X-Ca-alginate aerogels affect not only their material properties but other physical properties as well and hence their potential for different applications. For example, we have observed different sorption capacities for Pb^{2+} uptake from water samples by X-Ca-alg-RE (20.8 mg g^{-1})[19] and X-Ca-alg-N3300 (6.8 mg g^{-1})[61] under the same conditions. A detailed study on the behavior of X-Ca-alginate aerogels with other metal ions and in different environmental water samples is underway.

CONCLUSIONS

Polyurea-cross-linked Ca-alginate (X-Ca-alginate) aerogels show distinct nanoscale morphologies depending on the choice of the cross-linking triisocyanate reagent. Cross-linking native Ca-alginate wet gels with the aliphatic triisocyanate Desmodur N3300 yields aliphatic/flexible polyurea macromolecules in the final aerogel framework, while the aromatic triisocyanate Desmodur RE yields aromatic/rigid polyurea macromolecules. Probing the native Ca-alginate aerogel together with the polyurea-cross-linked X-Ca-alg-N3300 and X-Ca-alg-RE aerogels using LV SEM, N_2-sorption porosimetry, and contrast variation SANS enabled the reconstruction of the nanomorphology of the aerogels. Native Ca-alginate aerogels are built from primary nanoparticles (8.3 nm in radius) that aggregate in mass-fractal secondary particles. Cross-linking reactions are realized after the formation of the Ca-alginate nanostructure, while the different polyureas attach in different ways to the primary Ca-alginate nanoparticles. Cross-linking with the flexible aliphatic Desmodur N3300 triisocyanate leads to the formation of a compact polyurea layer over the primary nanoparticles following the contours of the native Ca-alginate skeletal framework (8.8 nm in radius). On the other hand, the rigid aromatic Desmodur RE triisocyanate forms a more rigid and randomly oriented polymer structure that fills loosely the empty space between the primary nanoparticles (10 nm in radius) within the secondary particles. Overall, both processes leave the primary Ca-alginate structure practically undisturbed, while it does affect the structure at the most fundamental level,

https://doi.org/10.1021/acsanm.1c02072
ACS Appl. Nano Mater. XXXX, XXX, XXX−XXX

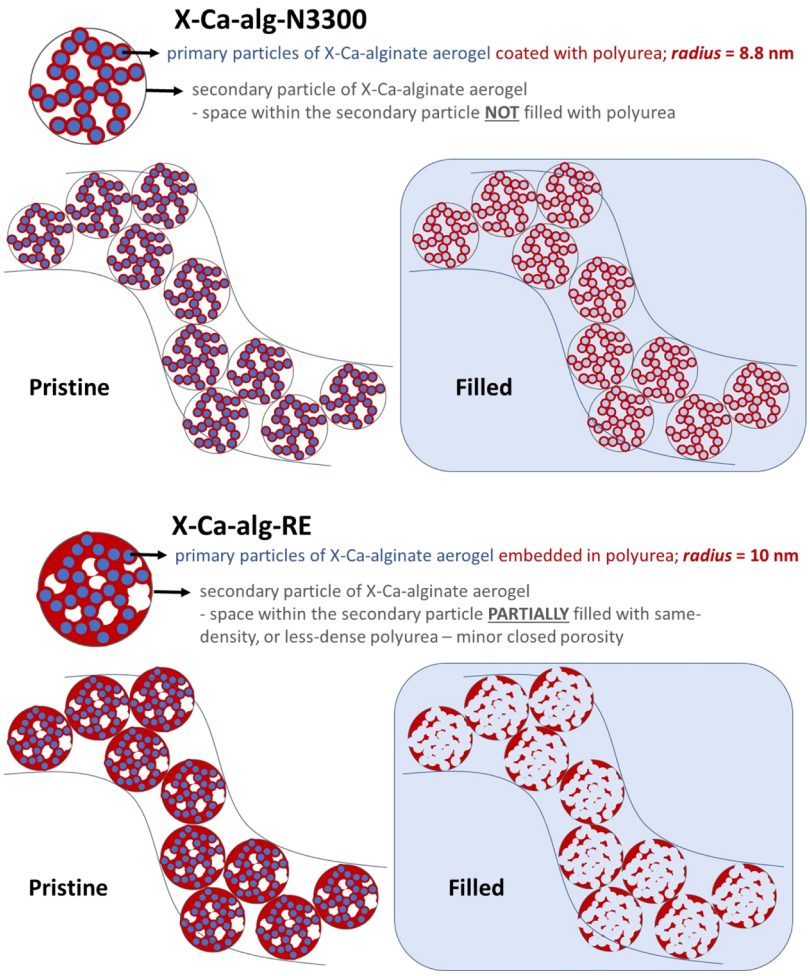

Figure 6. Proposed nanoscale structures of cross-linked (X-Ca-alg-N3300 and X-Ca-alg-RE) aerogels, as indicated. Panels labeled "filled" denotes filling with a contrast matching agent (a H_2O−D_2O mixture of 46 wt % H_2O−54 wt % D_2O) in SANS.

increasing the primary particle size and reducing the porosity. The different fundamental skeletal nanostructures of X-Ca-alginate aerogels affect not only their material properties but also their potential for application in environmental remediation.

AUTHOR INFORMATION

Corresponding Authors

Patrina Paraskevopoulou − *Inorganic Chemistry Laboratory, Department of Chemistry, National and Kapodistrian University of Athens, Athens 15771, Greece;* orcid.org/0000-0002-5166-8946; Email: paraskevopoulou@chem.uoa.gr

József Kalmár − *Department of Inorganic and Analytical Chemistry, MTA-DE Redox and Homogeneous Catalytic Reaction Mechanisms Research Group, University of Debrecen, Debrecen H-4032, Hungary;* orcid.org/0000-0002-2422-6106; Email: kalmar.jozsef@science.unideb.hu

Authors

Grigorios Raptopoulos − *Inorganic Chemistry Laboratory, Department of Chemistry, National and Kapodistrian University of Athens, Athens 15771, Greece*

Adél Len − *Neutron Spectroscopy Department, Centre for Energy Research, Budapest H-1121, Hungary*

Zoltán Dudás − *Neutron Spectroscopy Department, Centre for Energy Research, Budapest H-1121, Hungary*

István Fábián − *Department of Inorganic and Analytical Chemistry, MTA-DE Redox and Homogeneous Catalytic Reaction Mechanisms Research Group, University of Debrecen, Debrecen H-4032, Hungary;* orcid.org/0000-0002-4467-2912

Complete contact information is available at: https://pubs.acs.org/10.1021/acsanm.1c02072

Author Contributions

All authors have given approval to the final version of the manuscript.

Notes

The authors declare no competing financial interest.

ACKNOWLEDGMENTS

This research has been financially supported by the National Research, Development and Innovation Office, Hungarian Science Foundation (OTKA: FK_17-124571). J.K. is grateful for the János Bolyai Research Scholarship of the Hungarian Academy of Sciences and for the New National Excellence Program (ÚNKP-20-5 Bolyai+) of the Ministry of Innovation and Technology of Hungary for financial support. This research is cofinanced by Greece and the European Union (European Social Fund-ESF) through the Operational Programme "Human Resources Development, Education and Lifelong Learning" in the context of the project "Reinforcement of

Postdoctoral Researchers—Second Cycle" (MIS-5033021), implemented by the State Scholarships Foundation (IKY). Support from the Special Account of Research Grants of the National and Kapodistrian University of Athens is acknowledged. Work was carried out in the frame of the COST-Action "Advanced Engineering and Research of AeroGels for Environment and Life Sciences" (AERoGELS, ref. CA18125) funded by the European Commission. We are grateful to Covestro AG for kindly providing samples of Desmodur Ultra N3300 and Desmodur RE.

REFERENCES

(1) Leventis, N.; Sadekar, A.; Chandrasekaran, N.; Sotiriou-Leventis, C. Click Synthesis of Monolithic Silicon Carbide Aerogels from Polyacrylonitrile-Coated 3D Silica Networks. *Chem. Mater.* **2010**, *22*, 2790−2803.

(2) Vareda, J. P.; Lamy-Mendes, A.; Durães, L. A Reconsideration on the Definition of the Term Aerogel Based on Current Drying Trends. *Microporous Mesoporous Mater.* **2018**, *258*, 211−216.

(3) Kistler, S. S. Coherent Expanded Aerogels and Jellies. *Nature* **1931**, *127*, 741.

(4) Aegerter, M. A.; Leventis, N.; Koebel, M. M. *Aerogels Handbook*; Springer Science & Business Media, 2011.

(5) Stepanian, C. J.; Gould, G. L.; Begag, R. Aerogel Composite with Fibrous Batting. U.S. Patent 7,078,359 B2, July 18, 2006.

(6) Leventis, N. Three-Dimensional Core-Shell Superstructures: Mechanically Strong Aerogels. *Acc. Chem. Res.* **2007**, *40*, 874−884.

(7) Leventis, N.; Sotiriou-Leventis, C.; Zhang, G.; Rawashdeh, A.-M. M. Nanoengineering Strong Silica Aerogels. *Nano Lett.* **2002**, *2*, 957−960.

(8) Zhang, G.; Dass, A.; Rawashdeh, A.-M. M.; Thomas, J.; Counsil, J. A.; Sotiriou-Leventis, C.; Fabrizio, E. F.; Ilhan, F.; Vassilaras, P.; Scheiman, D. A.; McCorkle, L.; Palczer, A.; Johnston, J. C.; Meador, M. A.; Leventis, N. Isocyanate-Crosslinked Silica Aerogel Monoliths: Preparation and Characterization. *J. Non-Cryst. Solids* **2004**, *350*, 152−164.

(9) Mandal, C.; Donthula, S.; Far, H. M.; Saeed, A. M.; Sotiriou-Leventis, C.; Leventis, N. Transparent, Mechanically Strong, Thermally Insulating Cross-Linked Silica Aerogels for Energy-Efficient Windows. *J. Sol-Gel Sci. Technol.* **2019**, *92*, 84−100.

(10) Leventis, N.; Chandrasekaran, N.; Sadekar, A. G.; Sotiriou-Leventis, C.; Lu, H. One-Pot Synthesis of Interpenetrating Inorganic/Organic Networks of CuO/Resorcinol-Formaldehyde Aerogels: Nanostructured Energetic Materials. *J. Am. Chem. Soc.* **2009**, *131*, 4576−4577.

(11) Leventis, N.; Vassilaras, P.; Fabrizio, E. F.; Dass, A. Polymer Nanoencapsulated Rare Earth Aerogels: Chemically Complex but Stoichiometrically Similar Core−Shell Superstructures with Skeletal Properties of Pure Compounds. *J. Mater. Chem.* **2007**, *17*, 1502−1508.

(12) Rewatkar, P. M.; Soni, R. U.; Sotiriou-Leventis, C.; Leventis, N. A Cobalt Sunrise: Thermites Based on LiClO4-Filled Co(0) Aerogels Prepared from Polymer-Cross-Linked Cobaltia Xerogel Powders. *ACS Appl. Mater. Interfaces* **2019**, *11*, 22668−22676.

(13) Luo, H.; Churu, G.; Fabrizio, E. F.; Schnobrich, J.; Hobbs, A.; Dass, A.; Mulik, S.; Zhang, Y.; Grady, B. P.; Capecelatro, A.; Sotiriou-Leventis, C.; Lu, H.; Leventis, N. Synthesis and Characterization of the Physical, Chemical and Mechanical Properties of Isocyanate-Cross-linked Vanadia Aerogels. *J. Sol-Gel Sci. Technol.* **2008**, *48*, 113−134.

(14) Leventis, N.; Sotiriou-Leventis, C.; Mulik, S.; Dass, A.; Schnobrich, J.; Hobbs, A.; Fabrizio, E. F.; Luo, H.; Churu, G.; Zhang, Y.; Lu, H. Polymer Nanoencapsulated Mesoporous Vanadia with Unusual Ductility at Cryogenic Temperatures. *J. Mater. Chem.* **2008**, *18*, 2475−2482.

(15) Rewatkar, P. M.; Taghvaee, T.; Saeed, A. M.; Donthula, S.; Mandal, C.; Chandrasekaran, N.; Leventis, T.; Shruthi, T. K.; Sotiriou-Leventis, C.; Leventis, N. Sturdy, Monolithic SiC and Si3N4 Aerogels from Compressed Polymer-Cross-Linked Silica Xerogel Powders. *Chem. Mater.* **2018**, *30*, 1635−1647.

(16) Paraskevopoulou, P.; Smirnova, I.; Athamneh, T.; Papastergiou, M.; Chriti, D.; Mali, G.; Čendak, T.; Chatzichristidi, M.; Raptopoulos, G.; Gurikov, P. Mechanically Strong Polyurea/Polyurethane-Cross-Linked Alginate Aerogels. *ACS Appl. Polym. Mater.* **2020**, *2*, 1974−1988.

(17) Paraskevopoulou, P.; Smirnova, I.; Athamneh, T.; Papastergiou, M.; Chriti, D.; Mali, G.; Čendak, T.; Raptopoulos, G.; Gurikov, P. Polyurea-Crosslinked Biopolymer Aerogel Beads. *RSC Adv.* **2020**, *10*, 40843.

(18) Raptopoulos, G.; Papastergiou, M.; Chriti, D.; Effraimopoulou, E.; Čendak, T.; Samartzis, N.; Mali, G.; Ioannides, T.; Gurikov, P.; Smirnova, I.; Paraskevopoulou, P. Metal-Doped Carbons from Polyurea-Crosslinked Alginate Aerogel Beads. *Adv. Mater.* **2021**, *2*, 2684−2699.

(19) Paraskevopoulou, P.; Raptopoulos, G.; Leontaridou, F.; Papastergiou, M.; Sakellari, A.; Karavoltsos, S. Evaluation of Polyurea-Crosslinked Alginate Aerogels for Seawater Decontamination. *Gels* **2021**, *7*, 27.

(20) Baldino, L.; Zuppolini, S.; Cardea, S.; Diodato, L.; Borriello, A.; Reverchon, E.; Nicolais, L. Production of Biodegradable Superabsorbent Aerogels Using a Supercritical CO2 Assisted Drying. *J. Supercrit. Fluids* **2020**, *156*, 104681.

(21) Selmer, I.; Farrell, P.; Smirnova, I.; Gurikov, P. Comparison of Finite Difference and Finite Volume Simulations for a Sc-Drying Mass Transport Model. *Gels* **2020**, *6*, 45.

(22) Mißfeldt, F.; Gurikov, P.; Lölsberg, W.; Weinrich, D.; Lied, F.; Fricke, M.; Smirnova, I. Continuous Supercritical Drying of Aerogel Particles: Proof of Concept. *Ind. Eng. Chem. Res.* **2020**, *59*, 11284−11295.

(23) Selmer, I.; Behnecke, A.-S.; Quiño, J.; Braeuer, A. S.; Gurikov, P.; Smirnova, I. Model Development for Sc-Drying Kinetics of Aerogels: Part 1. Monoliths and Single Particles. *J. Supercrit. Fluids* **2018**, *140*, 415−430.

(24) Braeuer, A. S.; Gurikov, P.; Selmer, I.; Smirnova, I. Supercritical Drying of Aerogels: In Situ Raman Spectroscopy and Development of a Predictive Model. *Chem. Ing. Tech.* **2018**, *90*, 1207−1208.

(25) Posselt, D.; Pedersen, J. S.; Mortensen, K. SANS Investigation on Absolute Scale of a Homologous Series of Base-Catalysed Silica Aerogels. *J. Non-Cryst. Solids* **1992**, *145*, 128−132.

(26) Emmerling, A.; Fricke, J. Small Angle Scattering and the Structure of Aerogels. *J. Non-Cryst. Solids* **1992**, *145*, 113−120.

(27) Aristov, Y. I.; Lisitsa, N.; Zaikovski, V. I.; Lorenc, J.; Jarzebski, A. B. Fractal Structure in Base-Catalyzed Silica Aerogels Examined by TEM, SAXS and Porosimetry. *React. Kinet. Catal. Lett.* **1996**, *58*, 367−375.

(28) Craievich, A.; Aegerter, M. A.; dos Santos, D. I.; Woignier, T.; Zarzycki, J. A SAXS Study of Silica Aerogels. *J. Non-Cryst. Solids* **1986**, *86*, 394−406.

(29) Hasmy, A.; Foret, M.; Anglaret, E.; Pelous, J.; Vacher, R.; Jullien, R. Small-Angle Neutron Scattering of Aerogels: Simulations and Experiments. *J. Non-Cryst. Solids* **1995**, *186*, 118−130.

(30) Czakkel, O.; Marthi, K.; Geissler, E.; László, K. Influence of Drying on the Morphology of Resorcinol−Formaldehyde-Based Carbon Gels. *Microporous Mesoporous Mater.* **2005**, *86*, 124−133.

(31) Schaefer, D. W.; Pekala, R.; Beaucage, G. Origin of Porosity in Resorcinol-Formaldehyde Aerogels. *J. Non-Cryst. Solids* **1995**, *186*, 159−167.

(32) Reichenauer, G.; Emmerling, A.; Fricke, J.; Pekala, R. W. Microporosity in Carbon Aerogels. *J. Non-Cryst. Solids* **1998**, *225*, 210−214.

(33) Horikawa, T.; Hayashi, J.; Muroyama, K. Controllability of Pore Characteristics of Resorcinol−Formaldehyde Carbon Aerogel. *Carbon* **2004**, *42*, 1625−1633.

(34) Bock, V.; Emmerling, A.; Saliger, R.; Fricke, J. Structural Investigation of Resorcinol Formaldehyde and Carbon Aerogels Using SAXS and BET. *J. Porous Mater.* **1997**, *4*, 287−294.

(35) Fairén-Jiménez, D.; Carrasco-Marín, F.; Djurado, D.; Bley, F.; Ehrburger-Dolle, F.; Moreno-Castilla, C. Surface Area and Microporosity of Carbon Aerogels from Gas Adsorption and Small- and

https://doi.org/10.1021/acsanm.1c02072
ACS Appl. Nano Mater. XXXX, XXX, XXX−XXX

Wide-Angle X-Ray Scattering Measurements. *J. Phys. Chem. B* **2006**, *110*, 8681−8688.
(36) Cohaut, N.; Thery, A.; Guet, J. M.; Rouzaud, J. N.; Kocon, L. The Porous Network in Carbon Aerogels Investigated by Small Angle Neutron Scattering. *Carbon* **2007**, *45*, 1185−1192.
(37) Pahl, R.; Bonse, U.; Pekala, R. W.; Kinney, J. H. SAXS Investigations on Organic Aerogels. *J. Appl. Crystallogr.* **1991**, *24*, 771−776.
(38) Barbieri, O.; Ehrburger-Dolle, F.; Rieker, T. P.; Pajonk, G. M.; Pinto, N.; Venkateswara Rao, A. Small-Angle X-Ray Scattering of a New Series of Organic Aerogels. *J. Non-Cryst. Solids* **2001**, *285*, 109−115.
(39) Bock, V.; Emmerling, A.; Fricke, J. Influence of Monomer and Catalyst Concentration on RF and Carbon Aerogel Structure. *J. Non-Cryst. Solids* **1998**, *225*, 69−73.
(40) Leventis, N.; Sotiriou-Leventis, C.; Chandrasekaran, N.; Mulik, S.; Larimore, Z. J.; Lu, H.; Churu, G.; Mang, J. T. Multifunctional Polyurea Aerogels from Isocyanates and Water. A Structure−Property Case Study. *Chem. Mater.* **2010**, *22*, 6692−6710.
(41) Leventis, N.; Sotiriou-Leventis, C.; Saeed, A. M.; Donthula, S.; Majedi Far, H.; Rewatkar, P. M.; Kaiser, H.; Robertson, J. D.; Lu, H.; Churu, G. Nanoporous Polyurea from a Triisocyanate and Boric Acid: A Paradigm of a General Reaction Pathway for Isocyanates and Mineral Acids. *Chem. Mater.* **2016**, *28*, 67−78.
(42) Chidambareswarapattar, C.; Xu, L.; Sotiriou-Leventis, C.; Leventis, N. Robust Monolithic Multiscale Nanoporous Polyimides and Conversion to Isomorphic Carbons. *RSC Adv.* **2013**, *3*, 26459−26469.
(43) Chidambareswarapattar, C.; McCarver, P. M.; Luo, H.; Lu, H.; Sotiriou-Leventis, C.; Leventis, N. Fractal Multiscale Nanoporous Polyurethanes: Flexible to Extremely Rigid Aerogels from Multifunctional Small Molecules. *Chem. Mater.* **2013**, *25*, 3205−3224.
(44) Mohite, D. P.; Mahadik-Khanolkar, S.; Luo, H.; Lu, H.; Sotiriou-Leventis, C.; Leventis, N. Polydicyclopentadiene Aerogels Grafted with PMMA: II. Nanoscopic Characterization and Origin of Macroscopic Deformation. *Soft Matter* **2013**, *9*, 1531−1539.
(45) Berthon, S.; Barbieri, O.; Ehrburger-Dolle, F.; Geissler, E.; Achard, P.; Bley, F.; Hecht, A.-M.; Livet, F.; Pajonk, G. M.; Pinto, N.; Rigacci, A.; Rochas, C. DLS and SAXS Investigations of Organic Gels and Aerogels. *J. Non-Cryst. Solids* **2001**, *285*, 154−161.
(46) Forgács, A.; Papp, V.; Paul, G.; Marchese, L.; Len, A.; Dudás, Z.; Fábián, I.; Gurikov, P.; Kalmár, J. Mechanism of Hydration and Hydration Induced Structural Changes of Calcium Alginate Aerogel. *ACS Appl. Mater. Interfaces* **2021**, *13*, 2997−3010.
(47) Hu, X.; Littrel, K.; Ji, S.; Pickles, D. G.; Risen, W. M. Characterization of Silica−Polymer Aerogel Composites by Small-Angle Neutron Scattering and Transmission Electron Microscopy. *J. Non-Cryst. Solids* **2001**, *288*, 184−190.
(48) Rosa-Fox, N. d. l.; Morales-Flórez, V.; Toledo-Fernández, J. A.; Piñero, M.; Esquivias, L.; Keiderling, U. SANS Study of Hybrid Silica Aerogels under "in Situ" Uniaxial Compression. *J. Sol-Gel Sci. Technol.* **2008**, *45*, 245−250.
(49) Mohite, D. P.; Larimore, Z. J.; Lu, H.; Mang, J. T.; Sotiriou-Leventis, C.; Leventis, N. Monolithic Hierarchical Fractal Assemblies of Silica Nanoparticles Cross-Linked with Polynorbornene via ROMP: A Structure−Property Correlation from Molecular to Bulk through Nano. *Chem. Mater.* **2012**, *24*, 3434−3448.
(50) Woignier, T.; Primera, J.; Alaoui, A.; Dieudonne, P.; Duffours, L.; Beurroies, I.; Calas-Etienne, S.; Despestis, F.; Faivre, A.; Etienne, P. Fractal Structure in Silica and Composites Aerogels. *Gels* **2021**, *7*, 1.
(51) Lázár, I.; Forgács, A.; Horváth, A.; Király, G.; Nagy, G.; Len, A.; Dudás, Z.; Papp, V.; Balogh, Z.; Moldován, K.; Juhász, L.; Cserháti, C.; Szántó, Z.; Fábián, I.; Kalmár, J. Mechanism of Hydration of Biocompatible Silica-Casein Aerogels Probed by NMR and SANS Reveal Backbone Rigidity. *Appl. Surf. Sci.* **2020**, *531*, 147232.
(52) Salomonsen, T.; Jensen, H. M.; Larsen, F. H.; Steuernagel, S.; Engelsen, S. B. Alginate Monomer Composition Studied by Solution- and Solid-State NMR − A Comparative Chemometric Study. *Food Hydrocolloids* **2009**, *23*, 1579−1586.
(53) Juhász, L.; Moldován, K.; Gurikov, P.; Liebner, F.; Fábián, I.; Kalmár, J.; Cserháti, C. False Morphology of Aerogels Caused by Gold Coating for SEM Imaging. *Polymers* **2021**, *13*, 588.
(54) Hammouda, B. Analysis of the Beaucage Model. *J. Appl. Crystallogr.* **2010**, *43*, 1474−1478.
(55) Beaucage, G. Approximations Leading to a Unified Exponential/Power-Law Approach to Small-Angle Scattering. *J. Appl. Crystallogr.* **1995**, *28*, 717−728.
(56) Kline, S. R. Reduction and Analysis of SANS and USANS Data Using IGOR Pro. *J. Appl. Crystallogr.* **2006**, *39*, 895−900.
(57) Hou, L.; Wu, P. Exploring the Hydrogen-Bond Structures in Sodium Alginate through Two-Dimensional Correlation Infrared Spectroscopy. *Carbohydr. Polym.* **2019**, *205*, 420−426.
(58) Otsuki, A.; De Campo, L.; Garvey, C.; Rehm, C. H_2O/D_2O Contrast Variation for Ultra-Small-Angle Neutron Scattering to Minimize Multiple Scattering Effects of Colloidal Particle Suspensions. *Colloids Interfaces* **2018**, *2*, 37.
(59) Jeffries, C. M.; Graewert, M. A.; Blanchet, C. E.; Langley, D. B.; Whitten, A. E.; Svergun, D. I. Preparing Monodisperse Macromolecular Samples for Successful Biological Small-Angle X-Ray and Neutron-Scattering Experiments. *Nat. Protoc.* **2016**, *11*, 2122−2153.
(60) Kéri, M.; Forgács, A.; Papp, V.; Bányai, I.; Veres, P.; Len, A.; Dudás, Z.; Fábián, I.; Kalmár, J. Gelatin Content Governs Hydration Induced Structural Changes in Silica-Gelatin Hybrid Aerogels − Implications in Drug Delivery. *Acta Biomater.* **2020**, *105*, 131−145.
(61) Zoi, A.; Karanika, E. A. Diploma Thesis, Department of Chemistry, National and Kapodistrian University of Athens, Greece, 2021.

https://doi.org/10.1021/acsanm.1c02072
ACS Appl. Nano Mater. XXXX, XXX, XXX−XXX